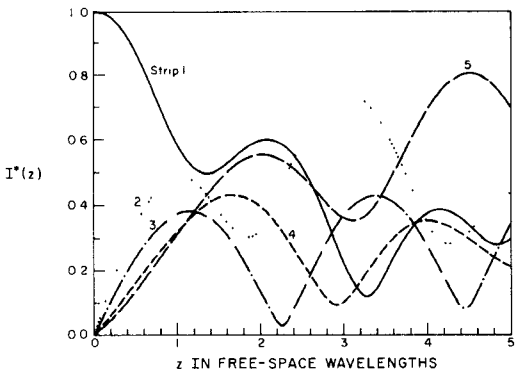

Fig. 8. Variation of I^* as a function of z at 1 GHz.

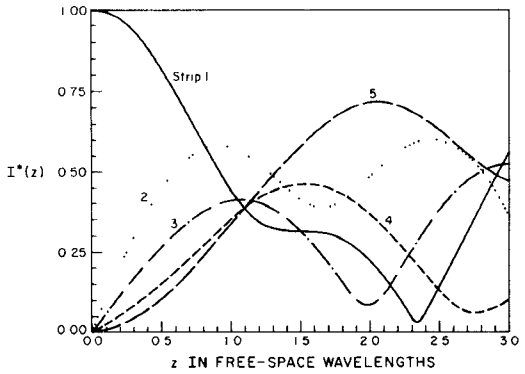

Fig. 9. Variation of I^* as a function of z at 10 GHz.

the modes at 1 GHz for a three-line configuration using both the spectral Galerkin and the quasi-static approaches, and a comparison is made in Table I. At this comparatively low frequency, the two methods are in excellent agreement. At higher frequencies, however, the quasi-static method is expected to break down, since it is a frequency-independent theory, and the propagation constants will be constant with respect to frequency.

This point is demonstrated in Fig. 2, where the five propagation constants of a five-strip system are plotted as a function of frequency. At low frequencies, the curves are level, as would be expected by quasi-static theory. At higher frequencies, however, the propagation constants are no longer constant, indicating that a frequency-dependent theory is now necessary.

Next, we checked the convergence of the calculated propagation constants with respect to the number of modes. These results, shown in Table II, demonstrate a very rapid convergence with respect to the number of modes and suggest that probably one basis function of each type ($N_z = N_x = 1$) will be sufficient for most calculations.

In order to get a physical feel for the shape of the five modes, we have plotted J_z as a function of x over a cross section of the strip for each of the five modes. These are shown in Figs. 3–7 for $N_z = N_x = 1$ (dotted line) and for $N_z = N_x = 3$ (solid line). We note that for most of he modes, we may obtain a very reasonable representation of the currents with just one basis function of each type.

Finally, we demonstrate the coupling of current from one strip to the next. In Fig. 8, we present results for the configuration of Fig. 1 at 1 GHz, and in Fig. 9 at 10 GHz. We start with a unit excitation on one of the end strips, say the first one from the left, and note that the current on the first strip very rapidly decreases, while the current on the other strips rapidly increases. Thus, when microstrips are closely spaced, the coupling between strips is predicted to be quite large.

V. Conclusions

In this paper, a frequency-dependent method of calculating the coupling between a large number of parallel microstrips has been demonstrated. Using this method, it has been shown that coupling between closely spaced lines can be quite severe. This has significance in the area of VLSI interconnectivity, where microstrip lines are packed as densely as possible.

References

[1] H. A. Wheeler, "Transmission-line properties of parallel strips separated by a dielectric sheet," *IEEE Trans Microwave Theory Tech.*, vol. MTT-13, pp. 172–185, Mar. 1965.

[2] T. G Bryant and J. A. Weiss, "Parameters of microstrip transmission lines and of coupled pairs of microstrip lines," *IEEE Trans. Microwave Theory Tech.*, vol. MTT-16, pp. 1021–1027, Dec. 1968.

[3] E. Yamashita and R Mittra, "Variational method for the analysis of microstrip lines," *IEEE Trans. Microwave Theory Tech.*, vol. MTT-16, pp. 251–256, Apr. 1968.

[4] Y. Rahmat-Samii, T. Itoh, and R Mittra, "A spectral domain technique for solving coupled microstrip line problems," *Arch. Elek. Übertragung.*, vol. 27, pp. 69–71, Feb. 1973.

[5] F. Y. Chang, "Transient analysis of lossless coupled transmission lines in a nonhomogeneous dielectric medium," *IEEE Trans. Microwave Theory Tech.*, vol. MTT-18, pp. 616–626, Sept. 1970.

[6] C. W. Ho, "Theory and computer-aided analysis of lossless transmission lines," *IBM J. Res. Develop.*, vol. 17, pp. 249–255, May 1973.

[7] J. Chilo and T. Arnaud, "Coupling effects in the time domain for an interconnecting bus in high speed GaAs logic circuits," *IEEE Trans. Electron Devices*, vol. ED-31, pp. 347–352, Mar. 1984.

[8] Cao Wei *et al.*, "Multiconductor transmission lines in multilayered dielectric media," *IEEE Trans. Microwave Theory Tech.*, vol. MTT-32, pp. 439–449, Apr. 1984

[9] C. Chan and R. Mittra, "Spectral iterative techniques for analyzing multiconductor microstrip lines," in *IEEE MTT Symp. Dig.*, May 1984, pp. 463–465.

[10] L.-P. Schmidt and T. Itoh, "Spectral domain analysis of dominant and higher order modes in fin-lines," *IEEE Trans. Microwave Theory Tech.*, vol. MTT-28, pp. 981–985, Sept. 1980.

[11] D. Mirshekar-Syahkal and J. Brian Davies, "Accurate solution of microstrip and coplanar structures for dispersion and for dielectric and conductor losses," *IEEE Trans. Microwave Theory Tech* , vol MTT-27, pp. 694–699, July 1979.

[12] T. Itoh, "Spectral domain immitance approach for dispersion characteristics of generalized printed transmission lines," *IEEE Trans Microwave Theory Tech.*, vol MTT-28, pp. 733–736, July 1980.

[13] P. Bhartia and I. J. Bahl, *Millimeter Wave Engineering and Applications*. New York: Wiley, 1984, pp. 379–380.

Comparison of Absorption Loss in Metal-Clad Optical Waveguides

S. J. AL-BADER AND H. A. JAMID

***Abstract*—A comparison of the absorption loss performance of three types of metal-clad slab waveguides is made with the material and waveguide properties standardized. The basic three-layer configuration of the step-index waveguide and two graded-index waveguides is considered; the latter two are also considered as two-layer structures. The comparative loss**

Manuscript received April 25, 1985, revised October 9, 1985.

The authors are with the Department of Electrical Engineering, University of Petroleum and Minerals, Dhahran, Saudi Arabia.

IEEE Log Number 8406448.

behavior is discussed from the point of view of application in mode and polarization filtering.

I. Introduction

Metal-clad waveguides are important in integrated optics because of the variety of functions that they offer. Most frequently, the inclusion of metals into optical circuits is such that the metals act as electrodes. However, metal-clad waveguides are also of interest as mode filters and polarizers in other applications. Two types of metal-clad slab waveguides have been studied in their basic configuration, i.e., as three-layer structures with the metal-cladding forming one of the layers. These are the step-index slab waveguides (SISW) [1]–[4], and the graded-index slab waveguides (GISW) [5]–[7]. The important features have been the loss performance of TE and TM modes and, in particular, the dependence of the loss of guided modes on the mode order and waveguides depth. The results show that the attenuation of TM modes is approximately an order of magnitude greater than that of TE modes and that the dependence of loss on the waveguides for the SISW is different from that of GISW. In particular, for a SISW of depth a, the loss varies as a^{-3} and for a GISW with a linearly graded layer it varies as a^{-1}, while for the GISW with a parabolic layer the loss varies with $a^{-3/2}$. The results also indicate that the loss behavior exhibits dependence on mode order for most waveguides, and on the index profile in the case of GISW.

Although most of the reported results are obtained for the wavelength 0.6328 μm, different material and waveguide parameters are generally used, making it difficult to establish a quantitative comparison of loss performance. It is thus of interest to compare the loss of SISW's and GISW's when material and waveguide properties are standardized. In this work, the loss of the SISW is compared with that of two types of GISW's, one having a linearly graded layer and the other a parabolic layer. The GISW's serve as models of waveguides obtained by diffusion with the two profiles being first approximations to the complementary error function and the Gaussian profiles, respectively.

In order to illustrate the role of the basic waveguide parameters in determining the loss, all waveguides are considered in their basic three-layer configurations. However, the GISW's are also considered as two-layer structures by allowing the graded regions to extend to infinity. Such models are easier to describe analytically and are shown here to give accurate results of loss for well-guided modes.

Finally, a comparison of expected performance of all three types of waveguides in applications in mode and polarization filtering is made in light of their ohmic loss characteristics. Throughout the work, scatter losses are neglected.

II. Theory

With a being the depth of the slab waveguide, the refractive-index distributions of the three waveguides considered are given below.

1) Step:

$$\begin{aligned} n^2(x) &= n_m^2, && x<0 \\ &= n_0^2, && 0<x<a \\ &= n_2^2, && x>a. \end{aligned} \tag{1}$$

2) Linear Layer:

$$\begin{aligned} n^2(x) &= n_m^2, && x>0 \\ &= n_0^2\left[1+2\Delta\left(\frac{x}{a}\right)\right], && -a<x<0 \\ &= n_2^2, && x<-a. \end{aligned} \tag{2}$$

3) Parabolic Layer:

$$\begin{aligned} n^2(x) &= n_m^2, && x<0 \\ &= n_0^2\left[1-2\Delta\left(\frac{x}{a}\right)^2\right], && 0<x<a \\ &= n_2^2, && x>a. \end{aligned} \tag{3}$$

Only the refractive index of the metal cladding n_m is taken to be complex and written as $n_m^2 = n_m'^2 + in_m''^2$. This notation is also used for the propagation constant $\beta = kn_{\text{eff}}$, so that $\beta^2 = \beta'^2 + i\beta''^2$ and $n_{\text{eff}}^2 = n_{\text{eff}}'^2 + in_{\text{eff}}''^2$. Equations (2) and (3) describe the GISW's with the graded layer truncated. When these are analyzed as two-layer structures, the graded layers are allowed to extend to infinity in one direction so that the truncations of $x=-a$ for model 2) and $x=a$ for model 3) are removed. The eigenequations of the different waveguide models are derived from the scalar wave equation after the imposition of appropriate boundary conditions. Details of the derivation are found in the literature [3], [5], [8], and only the necessary relationships are given here. It is assumed that all the time-harmonic field quantities are uniform in the y-direction.

In the numerical results section that follows, the eigenequations are solved by Muller's algorithm [9] with the eigenvalues corresponding to attenuated fields in the Z-direction. The eigen equations for the three waveguides under consideration are as follows.

1) Step:

$$(Q^2 - PR)\sin aQ = Q(P+R)\cos aQ, \quad \text{for TE modes} \tag{4}$$

$$\left(n_2^2 n_m^2 Q^2 - n_0^4 PR\right)\sin aQ = Qn_0^2\left(Pn_m^2 + Rn_2^2\right)\cos aQ, \quad \text{for TM modes} \tag{5}$$

2) Linear Layer:

$$\frac{SA_l'(-\xi_0) - RA_l(-\xi_0)}{SA_l'(-\xi_a) + PA_l(-\xi_a)} = \frac{SB_l'(-\xi_0) - RB_l(-\xi_0)}{SB_l'(-\xi_a) + PB_l(-\xi_a)}, \quad \text{for TE modes} \tag{6}$$

$$\frac{SA_l'(-\xi_0) - \left(\dfrac{Rn_0^2}{n_m^2} + \dfrac{\Delta}{a}\right)A_l(-\xi_0)}{SA_l'(-\xi_a) + \left(P - \dfrac{n_0\Delta}{an_2}\right)A_l(-\xi_a)} = \frac{SB_l'(-\xi_0) - \left(\dfrac{Rn_0^2}{n_m^2} + \dfrac{\Delta}{a}\right)B_l(-\xi_0)}{SB_l'(-\xi_a) + \left(P - \dfrac{n_0\Delta}{an_2}\right)B_l(-\xi_a)}, \quad \text{for TM modes.} \tag{7}$$

For the extended linear layer waveguide, (6) and (7) reduce to the following two equations:

$$SA_l'(-\xi_0) = RA_l(-\xi_0), \quad \text{for TE modes} \tag{8}$$

and

$$SA_l'(-\xi_0) = \left(\frac{Rn_0^2}{n_m^2} + \frac{\Delta}{a}\right)A_l(-\xi_0), \quad \text{for TM modes} \tag{9}$$

where A_l and B_l are the Airy functions.

3) Parabolic Layer:

$$k\chi^{1/2}\left[D_\nu'(\psi_a)-\frac{k\chi^{1/2}-\rho \mathrm{RF}}{k\chi^{1/2}+\rho \mathrm{RF}}D_\nu'(-\psi_a)\right] = -P\left[D_\nu(\psi_a)+\frac{k\chi^{1/2}-\rho \mathrm{RF}}{k\chi^{1/2}+\rho \mathrm{RF}}D_\nu(-\psi_a)\right],$$

for TE & TM modes (10)

where D_ν are the parabolic cylinder functions. For the extended parabolic layer waveguide, (10) can be shown to reduce to [7]

$$\frac{\Gamma\left(\frac{-\nu}{2}\right)}{\Gamma\left(\frac{1-\nu}{2}\right)}=\frac{(2\chi^{1/2})k}{R\rho}. \tag{11}$$

In the above case, as in the case of the extended linear layer model, the parameter a serves as a measure of waveguide depth. The various quantities are defined by the following:

$$Q^2=k^2\left(n_0^2-n_{\mathrm{eff}}^2\right) \tag{12}$$

$$P^2=k^2\left(n_{\mathrm{eff}}^2-n_2^2\right) \tag{13}$$

$$R^2=k^2\left(n_{\mathrm{eff}}^2-n_m^2\right) \tag{14}$$

$$S=\left(2k^2n_0^2\Delta/a\right)^{1/3} \tag{15}$$

$$\xi_0=Q^2/S^2 \tag{16}$$

$$\xi_a=-P^2/S^2 \tag{17}$$

$$\chi=2n_0\sqrt{2\Delta}/ak \tag{18}$$

$$\nu=\frac{Q^2}{k^2\chi}-\frac{1}{2} \tag{19}$$

$$F=\frac{-\Gamma\left(\frac{-\nu}{2}\right)}{\sqrt{2}\,\Gamma\left(\frac{1-\nu}{2}\right)} \tag{20}$$

$$\psi_a=ka\chi^{1/2} \tag{21}$$

$$\rho=\begin{cases}1, & \text{for TE modes}\\ n_0^2/n_m^2, & \text{for TM modes}\end{cases} \tag{22}$$

The objective is to find the complex roots of (4)–(11).

III. Numerical Results and Discussion

All the results presented here are obtained for waveguides with the following parameters: $n_0^2=5.2941$, $n_2^2=5.2441$, and $n_m^2=-10.3-i1.0$, which corresponds to gold cladding at $\lambda=0.6328$ μm. The parameter of interest is β'', the imaginary part of the propagation constant. Above cutoff, the occurrence of this parameter is due to the complex nature of the metal refractive index, which also renders the eigenequations complex and makes an insight into the loss behavior other than through numerical means difficult. The known dependence of loss on waveguide depth for models 1)–3) is that their loss is proportional to a^{-3} [2], a^{-1} [5], and $a^{-3/2}$ [7], respectively. The variation of β'' of the first two TE and TM modes with waveguide depth is shown in Figs. 1–4. The different β'' values for the index profiles shown are due to the different values of the fractional mode energy penetrating the metal. Also shown in these figures is the variation of loss of the extended linear and parabolic layer models. It is observed that these models give accurate descriptions of loss for

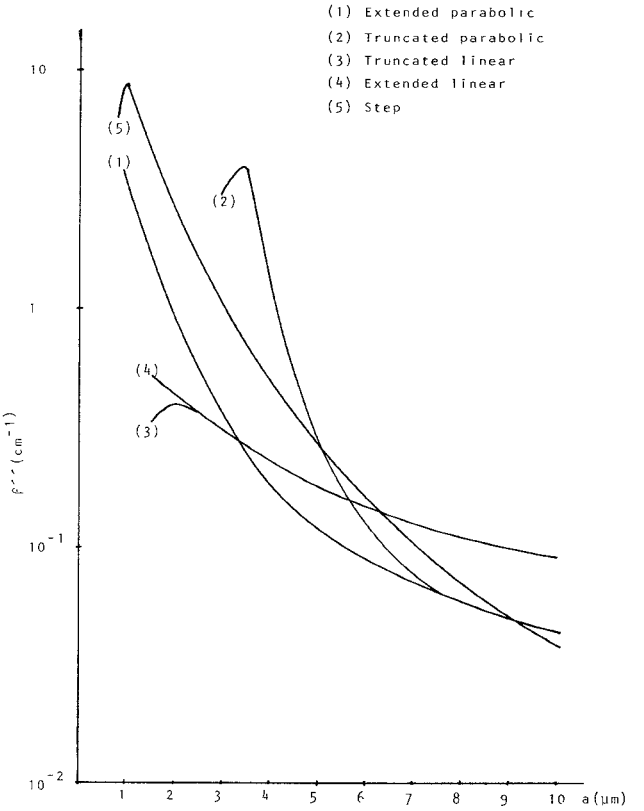

Fig. 1. β'' of the TE_0 mode.

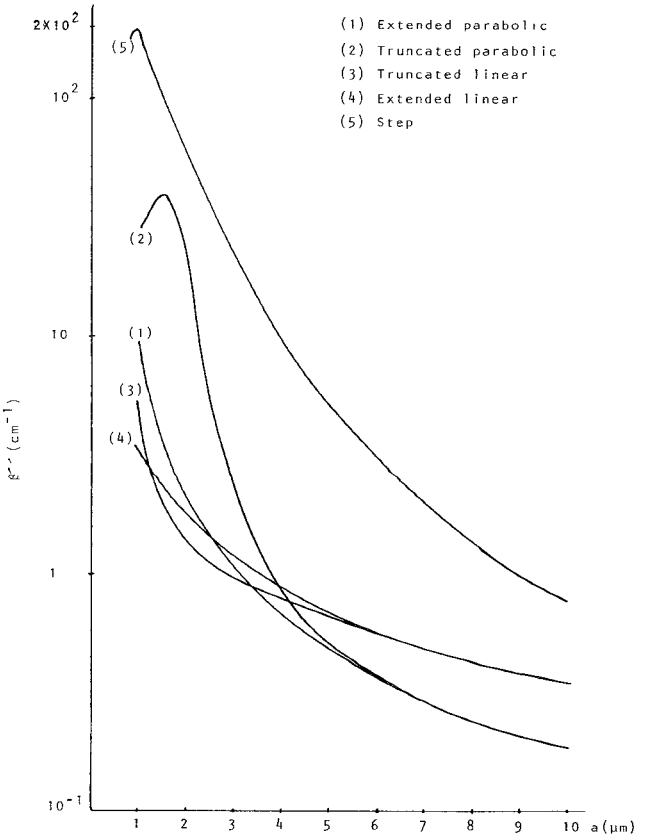

Fig. 2. β'' of the TM_0 mode.

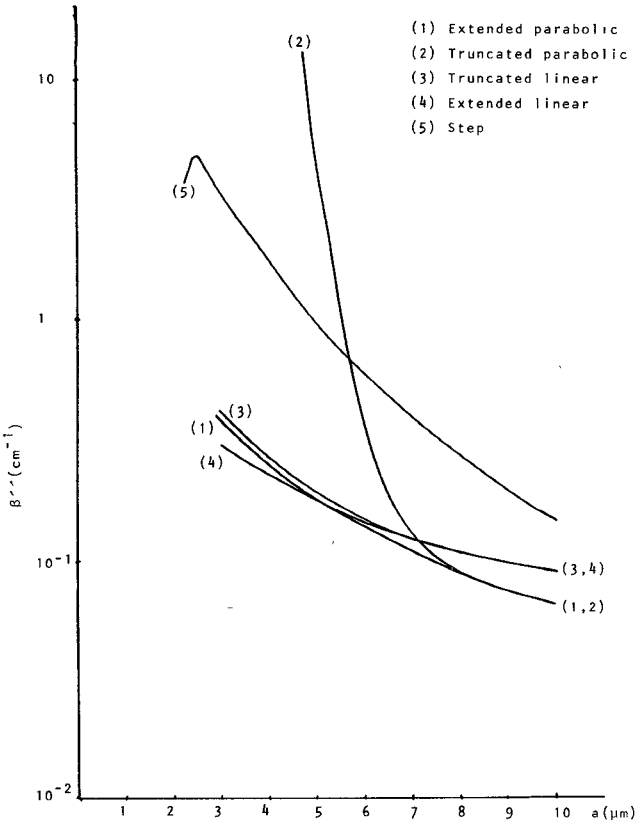

Fig. 3. β'' of the TE_1 mode.

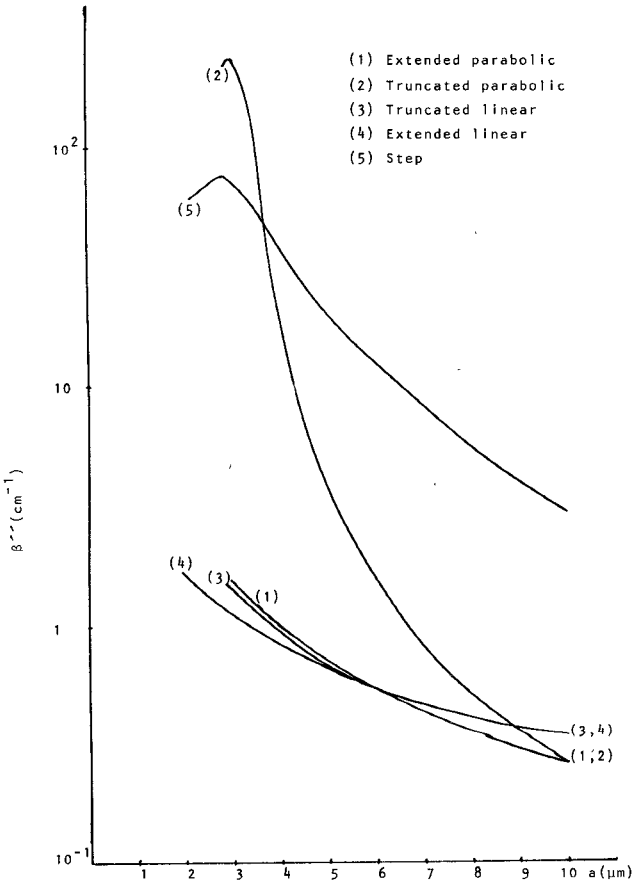

Fig. 4. β'' of the TM_1 mode.

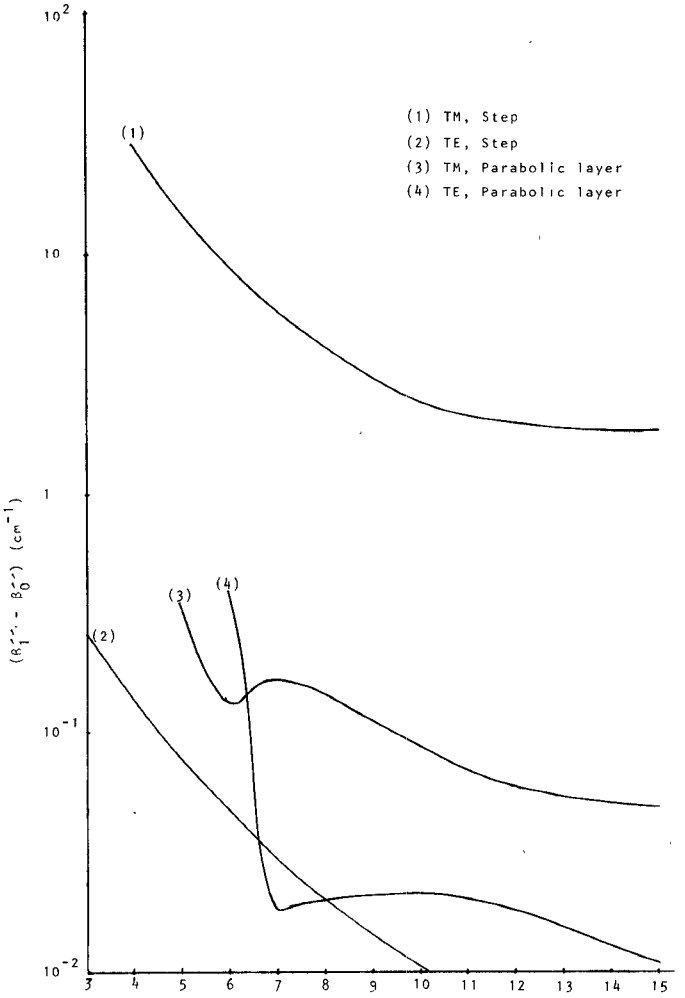

Fig. 5. Difference in the attenuation parameters of the two lowest order modes.

well-guided modes. The variation of the real part β' is not discussed here. However, it is noted that the metallic loss may be neglected in the evaluation of β'. Treatment of the lossless case for the relevant index profiles is found in [10].

The two features of interest are the mode discrimination and polarization discrimination performance of the three waveguides. In these respects, waveguide 2) is known to exhibit no loss dependence on mode order [5]. This property of the waveguide is well verified by the results of Figs. 1–4, and makes this waveguide unsuited for mode-filtering applications, where only low-order modes are required to pass. However, both waveguides 1) and 3) show mode dependence of loss. As a quantative measure of mode discrimination, the ratio of the amplitude of mode 1 to that of mode 0 is considered. The important parameter is $\beta_1''-\beta_0''$ of modes of the same polarization and is shown plotted against waveguide depth in Fig. 5. It is seen that the TM cases show higher discrimination than TE cases. This is to be expected as modal discrimination increases with modal loss. The SISW waveguide gives higher TM-mode discrimination than the parabolic layer waveguide, but the situation is reversed for well-guided TE modes. The accuracy of the results is checked by calculating the ratios β_1''/β_0'' of well-guided modes of the same polarization from Figs. 1–4. These are found to be 4 for waveguide 1) and 1.5 for waveguide 3): Both results verify theoretical calculations [4], [Appendix].

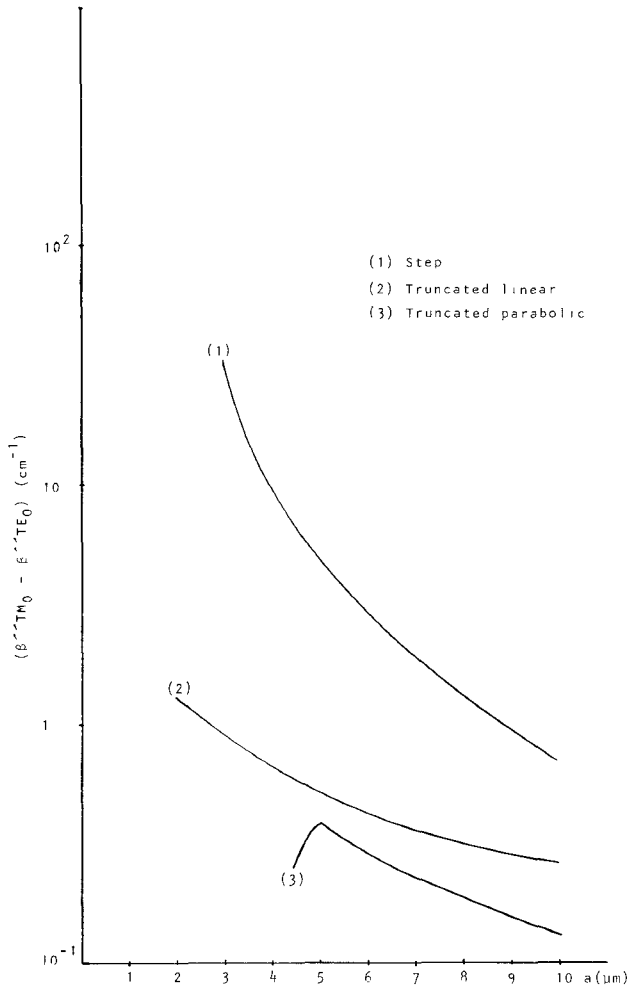

Fig. 6. Difference in the attenuation parameters of the lowest order TM and TE modes.

In a similar manner to the above, a measure of polarization discrimination is taken to be the ratio of the amplitudes of TM_0 modes to those of TE_0 modes. The important parameter in this case is $\beta''_{TM_0}-\beta''_{TE_0}$, which is shown plotted in Fig. 6. All three waveguides are seen to give polarization discrimination with the SISW having the highest ratio in the range of depth considered.

IV. Conclusions

The important loss mechanisms in slab waveguides are absorption and scatter processes with the latter having bulk and surface contributions. In applications utilizing loss, both mechanisms must be evaluated, and, thus, the application of both step-index and graded-index structures must be considered.

In mode-filtering applications, absorption-loss considerations show that the index profile of GISW's is an important design parameter. In particular, the quantity $\beta_1''-\beta_0''$ of guided TE and TM modes is positive for the SISW and the GISW with the parabolic layer, but is zero for the GISW with the linear layer. Published results indicate that this parameter becomes negative for the metal-clad waveguide with exponentially graded layer [6]. In the case of the present work, the largest values of $\beta_1''-\beta_0''$ are obtained with the SISW for TM modes and the GISW with the parabolic layer for TE modes in the range of waveguide depth considered. However, all three waveguides considered exhibit polarization discrimination with the SISW giving the largest values.

Appendix

In order to solve for n''_{eff} for the parabolic layer waveguide, the left-hand side of (11) is written in the expanded form [7]

$$\frac{\Gamma\left(\frac{-\nu}{2}\right)}{\Gamma\left(\frac{1-\nu}{2}\right)} = \frac{\Gamma\left(\frac{-\nu}{2}\right)\Gamma\left(1+\frac{\nu}{2}\right)}{\sqrt{\pi}} \cdot(1-\nu)\left(1+\frac{\nu}{2}\right)\left(1-\frac{\nu}{3}\right)\left(1+\frac{\nu}{4}\right)\cdots = \gamma + i\sigma\delta \tag{A1}$$

where for the purpose of derivation

$$\nu = \eta + i\delta = \frac{n_0^2 - n_{\text{eff}}^2}{\chi} - \frac{1}{2} \tag{A2}$$

with γ being the real part of the expansion and σ is a parameter to be calculated. By using the imaginary parts of (A1) and (A2) and the right-hand side of (11), we obtain

$$n''^2_{\text{eff}} = \frac{(2\chi^3)^{1/2}}{\sigma}\,\text{Im}\left[\frac{1}{(n_{\text{eff}}^2 - n_m^2)\rho}\right]. \tag{A3}$$

Observing that the right-hand side of (11) is much smaller than unity for the cases of interest, η is assumed to take up the values of $1,3,5\cdots$, i.e., those corresponding to the singularities of $\Gamma((1-\nu)/2)$ in the lossless case. Substituting from (A2) for ν into (A1), the parameter σ is found to order δ where $\delta \ll 1$. The values of σ for the first five lowest order modes are found to be: $\sqrt{\pi}$, 1.18194, 0.94530, 0.81026, 0.72023. Calculation of n''_{eff} from (A3) is completed by noting that $n''^2_{\text{eff}} \approx n_0^2$.

Acknowledgment

The authors would like to thank the University of Petroleum & Minerals, Dhahran, Saudi Arabia, for providing the facilities.

References

[1] E M Garmire and H. Stroll, "Propagation losses in metal-film-substrate optical waveguides," *IEEE J. Quant. Electron.*, vol. QE-8, pp 763-766, Oct. 1972
[2] A. Reisinger, "Attenuation properties of optical waveguides with a metal boundary," *Appl. Phys. Lett.*, vol. 23, pp. 237-239, Sept. 1973
[3] I. P Kaminow *et al.*, "Metal-clad optical waveguides: Analytical and experimental study," *Appl Optics*, vol. 13, pp. 396-405, Feb. 1974
[4] A. Reisinger, "Characteristics of optical guided modes in lossy waveguides," *Appl. Optics*, vol 12, pp 1015-1025, May 1973.
[5] M. Masuda *et al.*, "Propagation losses of guided modes in an optical graded-index slab waveguide with metal cladding," *IEEE Trans. Microwave Theory Tech* , vol. MTT-25, pp. 773-776, Sept. 1977.
[6] T. Findakley and C.-L. Chen, "Diffused optical waveguides with exponential profile: Effects of metal clad and dielectric overlay," *Appl. Optics*, vol. 17, pp. 469-474, Feb. 1978.
[7] S. J Al-Bader, "Ohmic loss in metal-clad graded-index optical waveguides," *IEEE J. Quant. Electron.*, Jan., 1986.
[8] I Ronchi *et al.*, "Wave propagation in a slab of transversely inhomogeneous medium, with gain or loss variations," *J. Opt. Soc. Am.*, vol. 70, pp. 191-197, Feb. 1980
[9] D. E. Muller, "A method for solving algebraic equations using an automatic computer," *MTAC*, vol. 10, pp. 208-215, 1956
[10] W. M Caton, "Propagation constants in diffused planar optical waveguides," *Appl. Opt.*, vol 13, pp 2755-2757, Dec. 1974.